RESEARCH ARTICLE | JULY 26 2023

Strain engineering in 2D hBN and graphene with evaporated thin film stressors

Ahmad Azizimanesh ; Aditya Dey ; Shoieb A. Chowdhury; Eric Wenner; Wenhui Hou ; Tara Peña ; Hesam Askari ; Stephen M. Wu

Appl. Phys. Lett. 123, 043504 (2023)
https://doi.org/10.1063/5.0153935

Applied Physics Letters ARTICLE pubs.aip.org/aip/apl

Strain engineering in 2D hBN and graphene with evaporated thin film stressors

Cite as: Appl. Phys. Lett. 123, 043504 (2023); doi: 10.1063/5.0153935
Submitted: 12 April 2023 · Accepted: 13 July 2023 ·
Published Online: 26 July 2023

Ahmad Azizimanesh,[1] Aditya Dey,[2] Shoieb A. Chowdhury,[2] Eric Wenner,[1] Wenhui Hou,[1] Tara Peña,[1] Hesam Askari,[2] and Stephen M. Wu[1,3,a)]

AFFILIATIONS

[1]Department of Electrical and Computer Engineering, University of Rochester, Rochester, New York 14627, USA
[2]Department of Mechanical Engineering, University of Rochester, Rochester, New York 14627, USA
[3]Department of Physics and Astronomy, University of Rochester, Rochester, New York 14627, USA

[a)]Author to whom correspondence should be addressed: stephen.wu@rochester.edu

ABSTRACT

We demonstrate a technique to strain two-dimensional hexagonal boron nitride (hBN) and graphene by depositing stressed thin films to encapsulate exfoliated flakes. We choose optically transparent stressors to be able to analyze strain in 2D flakes through Raman spectroscopy. Combining thickness-dependent analyses of Raman peak shifts with atomistic simulations of hBN and graphene, we can explore layer-by-layer strain transfer in these materials. hBN and graphene show strain transfer into the top four and two layers of multilayer flakes, respectively. hBN has been widely used as a protective capping layer for other 2D materials, while graphene has been used as a top gate layer in various applications. Findings of this work suggest that straining 2D heterostructures with evaporated stressed thin films through the hBN capping layer or graphene top contact is possible since strain is not limited to a single layer.

Two-dimensional (2D) materials offer a range of exceptional electrical, optical, and mechanical properties, making them a promising option for the development of advanced electronic or photonic circuits. These materials have various physical properties that are sensitive to strain and can be manipulated through mechanical strain.[1–4] Previously, straining 2D materials has been performed by macroscale techniques such as bending 2D flakes that are exfoliated onto flexible substrates,[5–7] creating ripples from exfoliation,[8] or by applying differential pressure to suspended membrane structures.[9] Nanoscale straining methods also exist, such as exfoliating 2D flakes onto nanopillars, nano-cones, or nano-indented substrates.[10–12] These techniques have large advantages in engineering nano/microscale strain in 2D systems but since deterministic device-by-device level control of strain is limited, all the previous methods have their limitations when applied to 2D systems on-chip in a densely integrated system.

Strain engineering has also been a key factor in the continued development of CMOS technology since the early 2000s, enhancing carrier mobility in individual transistors to overcome challenges in transistor scaling.[13–15] Utilizing the same strain engineering concepts used in Si-based transistor nanomanufacturing, process-induced strain engineering is also an effective method of straining 2D materials as well. Similar to stressor layers used in strained-Si CMOS technology,[16] stressed thin films that are deposited onto van der Waals (vdW) bonded 2D systems can cause strain transfer into the 2D materials due to the relaxation of stress inside the stressor layer.

In our previous work, we have fully explored strain engineering in 2D materials using evaporated stressed films. By uniformly depositing stressed films onto 2D flakes, the films cause uniform tensile or compressive biaxial strain to be transferred into the 2D material.[17] Using lithographic patterning of the stressors, we have shown that strain in 2D materials can be geometrically engineered by design for tension/compression, uniaxiality/biaxiality, and directionality relative to crystal axes on the micrometer-scale.[18] Moreover, we have shown that these strain engineering techniques are time and temperature stable, where the 2D flake stays strained for months and at all temperatures.[19] This method can be applied to various 2D materials on various substrates.

Previously, we have shown that in transition metal dichalcogenides (TMDs), such as MoS_2 and $MoTe_2$ using evaporated stressors, the achieved strain is not uniform in the out-of-plane direction and the strain has a specific transfer length-scale due to the weak out-of-plane vdW bonds.[20] Since interlayer interactions due to the vdW force are unique to each 2D material when utilizing process-induced strain

engineering techniques for other types of 2D materials and 2D heterostructures, a direct analysis of the strain transfer length-scale is required for each system. Here, we study the strain distribution properties in hexagonal boron nitride (hBN) and graphene, two of the most important and widely used 2D materials, to enable strain engineering in these materials and their twisted and non-twisted 2D heterostructures.

hBN is a wide bandgap 2D material with chemical stability and unique mechanical properties.[21,22] It has gained interest as an ideal substrate as well as a capping layer for other 2D materials, protecting them from oxidation, decay, and other environmental interactions.[23–25] Since hBN capping is widely employed in the fabrication of high-quality 2D heterostructures, straining 2D materials through the hBN capping layer becomes important. We show that strain engineering of 2D materials by depositing stressed thin films could be employed in heterostructures with an hBN protective layer since strain in the out-of-plane direction penetrates multiple layers.

Graphene has also been well studied since its discovery and has shown interesting electrical and mechanical properties.[26–29] Additionally, graphene has a variety of strain tunable properties,[30,31] and micrometer/nano-scale strain engineering in this material can create additional applications. Understanding the strain transfer length-scale in graphene will also allow for more complicated strain patterning of graphene-based vdW heterostructures, especially since graphene has been widely utilized as a top-gate electrode in many of these devices. Additionally, studying the strain distribution in the c-axis of different 2D materials (including graphene) becomes important since it makes it possible to engineer strain in individual layers (heterostrain) in a heterostructure with evaporated stressors on top.

Raman spectroscopy has been a reliable and useful tool to study strain in 2D materials.[5,32,33] Here, we focus on the E^{2g} Raman mode in hBN and G band in graphene to characterize strain in our samples to study strain distribution since these peaks have experimentally and theoretically shown the most sensitivity to biaxial in-plane strain.[34,35] In this work, we examine the strain transferred from the stressor into exfoliated hBN and graphene flakes on SiO_2/Si substrates. We have chosen to evaporate MgO as the stressor layer because of its reliable and reproducible compressive stress and its transparency to the 532 nm wavelength probe laser. This way, we may both apply strain to the 2D material and simultaneously probe it by Raman spectroscopy. See the supplementary material for details on the fabrication process, stress measurement, molecular statics (MS) modeling, and Raman study of stressor encapsulated samples.

The structure of the devices used in this work is presented in Fig. 1(a) where the exfoliated 2D flakes are fully coated with the stressor film, and the strain in coated devices is studied with Raman microscopy. Figure 1(b) illustrates the geometry of strained hBN samples where the red arrows show the distribution of strain magnitude in different layers. hBN flakes with thicknesses between 2L and 12L are coated with the stressor film. The Raman signatures of a 2L and a 4L device are presented in Fig. 1(c). As expected, the E^{2g} Raman mode (1368 $cm^{\bar{y}1}$) of hBN shifts down denoting tensile strain transfer into the 2D hBN flakes.

The same experiment is performed with graphene with the same thin film stressor layer as presented in Fig. 1(d). Raman signature of a 2L and a 4L graphene sample are presented in Fig. 1(e) where the downshift of G band (1580 $cm^{\bar{y}1}$) means that the flake is under tensile strain. An important observation in Figs. 1(c) and 1(e) is that the Raman peak shift in hBN and graphene is quite different between 2L and 4L, where a larger peak shift is observed in the bilayer of both materials. This hints that the strain distribution in the c-axis has a specific distribution in graphene and hBN and the few-layer flakes are not uniformly strained.

To understand the thickness-dependent distribution of strain, exfoliated hBN and graphene flakes with accurately identified thicknesses are required. Optical identification of flake thickness is a fast and reliable method that has been used for a variety of 2D materials.[36–38] We have identified the thickness of the hBN and graphene flakes using the optical contrast method and confirmed the thickness by atomic force microscopy and Raman spectroscopy. To increase the accuracy of thickness identification, the optical image of the flakes is split into three different color channels: red, blue, and green. The contrast of the flake is subtracted by the contrast of the background in each color channel, and the result is considered the actual color contrast of the flake. Figures 2(a) and 2(b) present the color contrasts for different thicknesses of hBN and graphene, respectively. Figures 2(a)

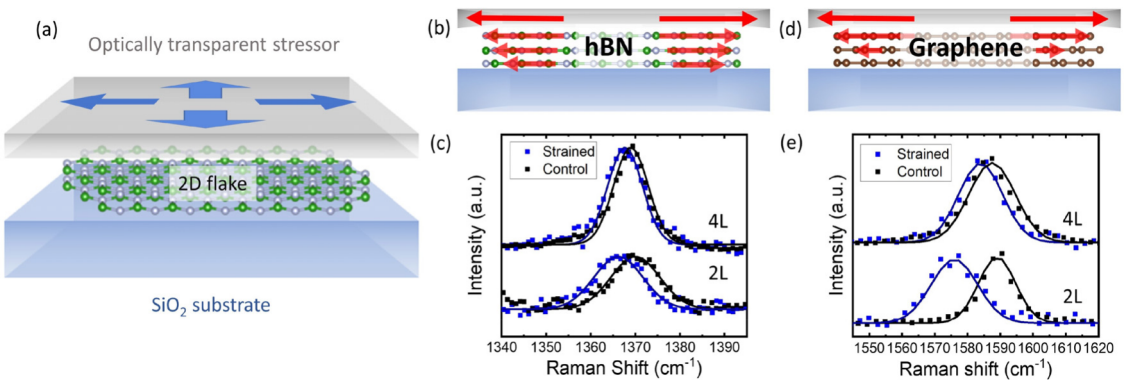

FIG. 1. (a) Evaporation of thin film stressors onto exfoliated hBN or graphene samples. (b) and (d) Visual representation of an evaporated compressive MgO stressor expanding to release stress within itself, leading to tensilely strained 2D flakes. The presented strain transfer (smaller red arrows) varies layer-by-layer. Raman spectra of 2 and 4L hBN (c) and graphene (e) samples demonstrating clear shifts in the E^{2g} and G band phonon modes. Blue spectrum is that of a strained hBN/graphene, black is a control exfoliated hBN/graphene.

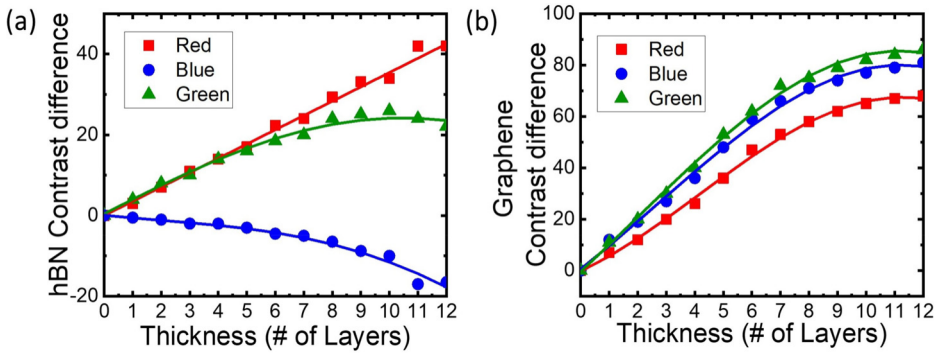

FIG. 2. (a) Contrast of red, blue, and green color channels of optical image for different thicknesses of hBN (a) and graphene (b) used to accurately identify flake thicknesses.

shows the most accurate color to identify the thickness of hBN flakes on the SiO_2 substrate, which is the red channel of the optical image that increases linearly with flake thickness. On the other hand, all color channels for graphene show linear relation with thickness, meaning each color channel can be used to identify the thickness of the flake.

The Raman peak position is extracted from the Raman signal of control and encapsulated flakes by fitting the peak with a Lorentzian function. Figure 3(a) presents the Raman peak position for control and strained hBN. The Raman peak position in hBN has an exponential relation with the number of layers. However, in strained hBN, the Raman peak position diverges from the control value as the flake gets thinner. It implies that the top few layers of hBN are strained, but due to the weak out-of-plane mechanical coupling among the layers, strain decays through the c-axis. The reason for this behavior is that the top layer of the flake regardless of the thickness is strained similarly but the Raman laser penetrates through the whole flake and the collected Raman signal is an average of the whole flake thickness. In other words, the Raman peak shift that is observed in each thickness shows the average strain in the whole 2D flake. In thicker flakes, the Raman signal of the strained top layers is averaged with the Raman signal of the unstrained bottom layers, and we see a smaller peak shift.

Figure 3(b) presents the G band Raman position for control and strained graphene flakes with various thicknesses. Similar to hBN, the Raman peak position in graphene also suggests a non-uniform strain distribution in the c-axis in multilayer graphene as the G band position diverges for thinner flakes. Comparing Figs. 3(a) and 3(b), it can be observed that the Raman peak position diverges at thicker samples in hBN, which hints that in hBN, the strain transfer length-scale is possibly longer than that in graphene, which could be due to the difference in out-of-plane vdW interaction in the two materials.

The Raman peak position in strained monolayer samples does not follow the same trend because the bottom layer is well-adhered to the substrate [Fig. 3(b)]. Hence, there will be only a negligible amount of strain transferred to the layer in contact with the substrate (i.e., monolayer) compared to the strain in the top layer of thicker flakes (Fig. S1). The fixed boundary condition is a prerequisite to engineering strain on 3D substrates, where otherwise complete delamination from the substrate will occur when stressors are deposited with poor substrate adhesion. This boundary condition can be relieved when the 2D material is placed upon a 2D substrate in a vdW heterostructure, where monolayers may then be strained freely. This behavior was first reported by our group when exploring strain transfer in MoS_2,[17] where monolayer MoS_2 is exfoliated onto hBN flakes and significantly strained using a similar type of evaporated stressor.

Doping hBN with impurities results in changes in intensity and FWHM of the Raman peaks and introduces new phonon modes such as the D and G modes.[39] We observed similar peak intensities and FWHMs of the E^{2g} mode in encapsulated and control bilayer hBN and no new Raman mode appears, which means the chosen stressor does not add a doping effect to the hBN flakes. In graphene, strain and doping have different effects on how the G and 2D Raman modes shift.[40] The Raman peak shift that we see in graphene is purely due to the strain and no detectable doping or defect from the stressor is observed in monolayer graphene encapsulated with the same stressor (Figs. S1 and S2).

To properly characterize the layer-by-layer nature of strain transfer in hBN and graphene, we perform atomistic simulations using a

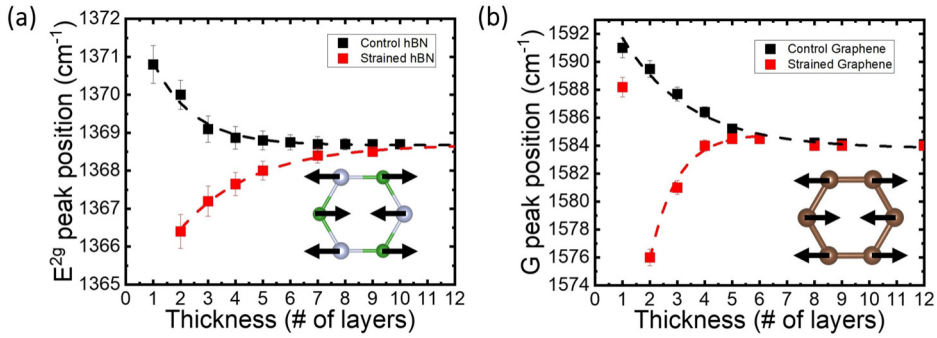

FIG. 3. (a) E^{2g} peak position as a function of strained (red) and control (black) hBN sample thickness. (b) G band peak position as a function of strained (red) and control (black) graphene sample thickness. Dashed lines in both figures exhibit fitted exponentials to each curve for clarity.

molecular statics (MS) approach. Atomistic models of stacked layers of graphene (Bernal stacking)[41] and hBN (AB stacking)[34] (2L–12L) were prepared. To mimic the experimental setup of strain engineering, an in-plane biaxial loading condition is applied to the top layer, replicating the fully encapsulated flakes while the bottom layer is fixed to the substrate and has no strain. The biaxial strain ($\varepsilon = \sqrt{\varepsilon_x^2 + \varepsilon_y^2}$) has a magnitude of 0.5%, below the interlayer slippage limit in these materials (0.53% in graphene and 0.68% in hBN[42,43]).

We obtain the strain distribution through the layers and subsequently extract the strain transfer length-scale across their thickness (along c-axis). The simulated atomistic models representing strain distributed throughout the sample are shown in Figs. 4(a) and 4(d), while Figs. 4(b) and 4(e) show the average strain within each layer for 2L–12L hBN and graphene samples, respectively. The calculated strain transfer magnitude is obtained by averaging the strain within the whole layer. By increasing the sample thickness in both materials, strain transferred to the layer beneath the top layer increases because as the sample gets thicker, the second layer is less impacted by the fixed bottom layer and is freer to be strained from the top. Moreover, we observe that strain penetrates significantly up to the top two layers in graphene and the top four layers in hBN, which implies the strain transfer length-scale is higher in hBN compared to graphene. Our findings indicate that approximately 60% and 30% of the strain applied to the top layer of hBN is observed in the second and third layers, respectively. Similarly, strain in graphene is not limited to the top layer and 40% of strain applied to the top layer of graphene is observed in the second layer.

To validate our computational findings, we further compare these results with experimentally obtained strain transfer length-scale via Raman peak measurements. Similar to our previous work on TMDs,[17,20] we first quantify translation factors in hBN and graphene that convert Raman peak shifts (cm^{-1}) to strain (%) from previous work on biaxial strain in hBN and graphene.[34,35] The Raman measurement of these samples obtained experimentally is a collective measure

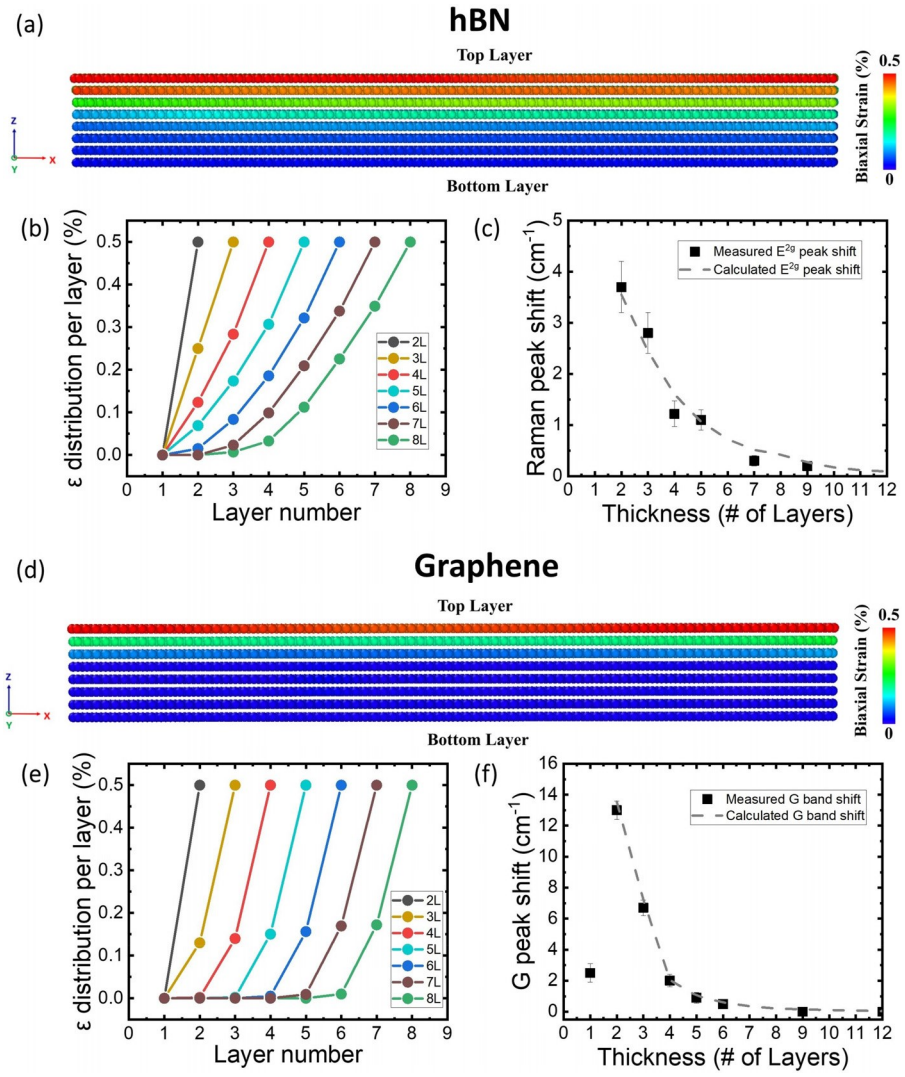

FIG. 4. (a) The strain distribution throughout an 8L sample of hBN from MS simulations. (b) Layer-by-layer strain distribution for various thicknesses of hBN determined from MS. (c) The calculated E^{2g} peak shifts (grey line) due to strain compared to measured E^{2g} peak shifts for various thicknesses in hBN extracted from Fig. 3(a). (d) The strain distribution throughout an 8L sample of graphene from MS simulations. (e) Layer-by-layer strain distribution for various thickness samples of graphene determined from MS. (f) The calculated G band peak shifts (grey line) due to strain compared to actual measured G band peak shifts for various thicknesses in graphene extracted from Fig. 3(b).

of optical responses from individual layers, which is superimposed to a single peak.[42,44] To calculate the expected Raman peak shift due to strain results from the theoretical model, we assume a fixed strain magnitude (%) in the top layer of different thicknesses and estimate the strain in other layers based on the data from Figs. 4(b) and 4(e) and assign a Raman peak with a Lorentzian function to each layer that is shifted with the corresponding amount of strain. We then superimpose the responses from each layer for each sample thickness to form a single Raman peak, then extract the peak position of the resulting response. Finally, the maximum strain in the top layer is adjusted to confirm that the exponential decay trend of the E^{2g} peak in the hBN and G band in graphene aligns with our experimental findings.

Figures 4(c) and 4(f) present the Raman peak shift due to strain for different thicknesses of hBN and graphene (extracted from Fig. 3) and the calculated Raman peak shift based on the simulated strain distribution. We confirm that the calculated exponential decay trend of DE^{2g} in hBN and DG band in graphene matches quite well with what we found experimentally. Additionally, the strain in the top layer of hBN and graphene is estimated to be 0.3% and 0.4%, respectively, by comparing the estimated top layer Raman peak shift with the translation factors.[34,35] The Youngs modulus of hBN and graphene are reported to be 0.86 and 1 TPa, respectively,[45] and when subjected to equal amounts of stress, graphene is expected to exhibit slightly more strain than hBN. The reason we are observing smaller strain in hBN is possibly that in bilayer and trilayer samples, the top layer is bonded to/affected by the fixed bottom layer and does not feel the same stress as in the top layer of bilayer or trilayer graphene.

The unique propagation of strain in the c-axis of 2D materials can be attributed to the weak out-of-plane bonding among layers of these materials that results in the incomplete transfer of shear traction between the layers.[17,46] Consequently, there is a decrease in the amount of traction felt by each successive layer of the 2D flake from the preceding layer, which is likely the explanation for the observed decay in strain in the out-of-plane direction of few-layered 2D flakes. Depending on the strength of interlayer bonding for different 2D materials, the transfer of traction varies, thus affecting the strain transfer propagation depth.

In this work, we have been able to show that with the deposition of stressed thin film, we can strain exfoliated 2D hBN and graphene. By studying the strain in different thicknesses of hBN and graphene flakes encapsulated with the same stressor film, we show that strain significantly penetrates two layers in the c-axis of multilayer graphene while penetrating four layers in multilayer hBN. The strain transfer length-scale reported here and previously in TMDs[20] is unique to each 2D material depending on interlayer vdW coupling. hBN and graphene are widely used as the top dielectric and top contact materials, respectively, in 2D vdW heterostructures. Knowing that strain is not limited to only one layer of hBN and graphene means straining 2D heterostructures with an hBN capping layer or a graphene top contact is possible using the method of thin film stressor deposition. This may open the possibility for control over a wide variety of strain-tunable 2D material properties in twisted and non-twisted graphene and hBN and their 2D heterostructures.

See the supplementary material for Raman spectra and further discussion on strain and doping effects in graphene, and details about the experimental and simulation methods.

We acknowledge support from the National Science Foundation (NSF) (Grant Nos. OMA-1936250 and ECCS-1942815) and the National Science Foundation Graduate Research Fellowship Program (Grant No. DGE-1939268). Raman spectroscopy was performed at the Cornell Center for Materials Research's (CCMR) Shared Facilities, and the CCMR is supported through the NSF MRSEC Program (Grant No. DMR-1719875).

AUTHOR DECLARATIONS

Conflict of Interest

The authors have no conflicts to disclose.

Author Contributions

Ahmad Azizimanesh and Aditya Dey contributed equally to this work.

Ahmad Azizimanesh: Conceptualization (equal); Data curation (equal); Formal analysis (equal); Investigation (equal); Methodology (equal); Writing – original draft (equal); Writing – review & editing (equal). Aditya Dey: Data curation (equal); Formal analysis (equal); Investigation (equal); Methodology (equal); Writing – original draft (equal); Writing – review & editing (equal). Shoieb A. Chowdhury: Data curation (equal); Investigation (equal); Writing – review & editing (equal). Eric Wenner: Data curation (equal); Investigation (equal). Wenhui Hou: Investigation (equal). Tara Peña: Investigation (equal). Hesam Askari: Funding acquisition (equal); Investigation (equal); Supervision (equal); Validation (equal); Writing – review & editing (equal). Stephen Mingda Wu: Conceptualization (equal); Funding acquisition (equal); Supervision (equal); Validation (equal); Writing – original draft (equal); Writing – review & editing (equal).

DATA AVAILABILITY

The data that support the findings of this study are available from the corresponding author upon reasonable request.

REFERENCES

[1]S. B. Desai, G. Seol, J. S. Kang, H. Fang, C. Battaglia, R. Kapadia, J. W. Ager, J. Guo, and A. Javey, Nano Lett. 14, 4592 (2014).
[2]S. Manzeli, A. Allain, A. Ghadimi, and A. Kis, Nano Lett. 15, 5330 (2015).
[3]H. Guo, N. Lu, L. Wang, X. Wu, and X. C. Zeng, J. Phys. Chem. C 118, 7242 (2014).
[4]Y. Ge, W. Wan, F. Yang, and Y. Yao, New J. Phys. 17, 035008 (2015).
[5]H. J. Conley, B. Wang, J. I. Ziegler, R. F. Haglund, S. T. Pantelides, and K. I. Bolotin, Nano Lett. 13, 3626 (2013).
[6]A. Castellanos-Gomez, R. Roldan, E. Cappelluti, M. Buscema, F. Guinea, H. S. J. van der Zant, and G. A. Steele, Nano Lett. 13, 5361 (2013).
[7]R. Yang, J. Lee, S. Ghosh, H. Tang, R. M. Sankaran, C. A. Zorman, and P. X. L. Feng, Nano Lett. 17, 4568 (2017).
[8]J. Quereda, P. San-Jose, V. Parente, L. Vaquero-Garzon, A. J. Molina-Mendoza, N. Agraït, G. Rubio-Bollinger, F. Guinea, R. Roldan, and A. Castellanos-Gomez, Nano Lett. 16, 2931 (2016).
[9]D. Lloyd, X. Liu, J. W. Christopher, L. Cantley, A. Wadehra, B. L. Kim, B. B. Goldberg, A. K. Swan, and J. S. Bunch, Nano Lett. 16, 5836 (2016).
[10]A. Reserbat-Plantey, D. Kalita, Z. Han, L. Ferlazzo, S. Autier-Laurent, K. Komatsu, C. Li, R. Weil, A. Ralko, L. Marty, and S. Gueron, Nano Lett. 14, 5044 (2014).
[11]H. Li, A. W. Contryman, X. Qian, S. M. Ardakani, Y. Gong, X. Wang, J. M. Weisse, C. H. Lee, J. Zhao, P. M. Ajayan, J. Li, H. C. Manoharan, and X. Zheng, Nat. Commun. 6, 7381 (2015).

[12]S. T. Gill, J. H. Hinnefeld, S. Zhu, W. J. Swanson, T. Li, and N. Mason, ACS Nano 9, 5799 (2015).
[13]S. E. Thompson, M. Armstrong, C. Auth, M. Alavi, M. Buehler, R. Chau, S. Cea, T. Ghani, G. Glass, T. Hoffman, C. H. Jan, C. Kenyon, J. Klaus, K. Kuhn, Z. Ma, B. Mcintyre, K. Mistry, A. Murthy, B. Obradovic, R. Nagisetty, P. Nguyen, S. Sivakumar, R. Shaheed, L. Shifren, B. Tufts, S. Tyagi, M. Bohr, and Y. El-Mansy, IEEE Trans. Electron Devices 51, 1790 (2004).
[14]J. L. Hoyt, H. M. Nayfeh, S. Eguchi, I. Aberg, G. Xia, T. Drake, E. A. Fitzgerald, and D. A. Antoniadis, Tech. Dig. - Int. Electron Devices Meet. 2002, 23–26.
[15]M. L. Lee, E. A. Fitzgerald, M. T. Bulsara, M. T. Currie, and A. Lochtefeld, J. Appl. Phys. 97, 011101 (2005).
[16]P. R. Chidambaram, C. Bowen, S. Chakravarthi, C. Machala, and R. Wise, IEEE Trans. Electron Devices 53, 944 (2006).
[17]T. Pena, S. A. Chowdhury, A. Azizimanesh, A. Sewaket, H. Askari, and S. M. Wu, 2D Mater. 8, 045001 (2021).
[18]A. Azizimanesh, T. Pena, A. Sewaket, W. Hou, and S. M. Wu, Appl. Phys. Lett. 118, 213104 (2021).
[19]T. Pena, A. Azizimanesh, L. Qiu, A. Mukherjee, A. N. Vamivakas, and S. M. Wu, J. Appl. Phys. 131, 024304 (2022).
[20]S. A. Chowdhury, K. Inzani, T. Pena, A. Dey, S. M. Wu, S. M. Griffin, and H. Askari, J. Eng. Mat. Technol. 144, 011006 (2022).
[21]D. Wickramaratne, L. Weston, and C. G. van de Walle, J. Phys. Chem. C 122, 25524 (2018).
[22]L. Boldrin, F. Scarpa, R. Chowdhury, and S. Adhikari, Nanotechnology 22, 505702 (2011).
[23]S. Pace, L. Martini, D. Convertino, D. H. Keum, S. Forti, S. Pezzini, F. Fabbri, V. Miseikis, and C. Coletti, ACS Nano 15, 4213 (2021).
[24]S. Larentis, B. Fallahazad, H. C. P. Movva, K. Kim, A. Rai, T. Taniguchi, K. Watanabe, S. K. Banerjee, and E. Tutuc, ACS Nano 11, 4832 (2017).
[25]S. Sinha, Y. Takabayashi, H. Shinohara, and R. Kitaura, 2D Mater. 3, 035010 (2016).
[26]M. J. Allen, V. C. Tung, and R. B. Kaner, Chem. Rev. 110, 132 (2010).
[27]C. N. R. Rao, A. K. Sood, K. S. Subrahmanyam, and A. Govindaraj, Angew. Chem. Int. Ed. 48, 7752 (2009).
[28]A. Nimbalkar and H. Kim, Nanomicro Lett. 12, 126 (2020).
[29]M. S. Cao, X. X. Wang, W. Q. Cao, and J. Yuan, J. Mater. Chem. C 3, 6589 (2015).
[30]C. Si, Z. Sun, and F. Liu, Nanoscale 8, 3207 (2016).
[31]S. M. Choi, S. H. Jhi, and Y. W. Son, Phys. Rev. B 81, 081407 (2010).
[32]W. Wang, Z. Li, A. J. Marsden, M. A. Bissett, and R. J. Young, 2D Mater. 8, 035058 (2021).
[33]Z. H. Ni, T. Yu, Y. H. Lu, Y. Y. Wang, Y. P. Feng, and Z. X. Shen, ACS Nano 2, 2301 (2008).
[34]C. Androulidakis, E. N. Koukaras, M. Poss, K. Papagelis, C. Galiotis, and S. Tawfick, Phys. Rev. B 97, 241414 (2018).
[35]C. Androulidakis, E. N. Koukaras, J. Parthenios, G. Kalosakas, K. Papagelis, and C. Galiotis, Sci. Rep. 5, 18219 (2015).
[36]H. Li, J. Wu, X. Huang, G. Lu, J. Yang, X. Lu, Q. Xiong, and H. Zhang, ACS Nano 7, 10344 (2013).
[37]H. Zhang, F. Ran, X. Shi, X. Fang, S. Wu, Y. Liu, X. Zheng, P. Yang, Y. Liu, L. Wang, X. Huang, H. Li, and W. Huang, Nanotechnology 28, 164001 (2017).
[38]Y. Y. Wang, R. X. Gao, Z. H. Ni, H. He, S. P. Guo, H. P. Yang, C. X. Cong, and T. Yu, Nanotechnology 23, 495713 (2012).
[39]S. Lu, P. Shen, H. Zhang, G. Liu, B. Guo, Y. Cai, H. Chen, F. Xu, T. Zheng, F. Xu, X. Chen, D. Cai, and J. Kang, Nat. Commun. 13, 3109 (2022).
[40]J. E. Lee, G. Ahn, J. Shim, Y. S. Lee, and S. Ryu, Nat. Commun. 3, 1024 (2012).
[41]E. McCann and M. Koshino, Rep. Prog. Phys. 76, 056503 (2013).
[42]H. Wang, Y. Wang, X. Cao, M. Feng, and G. Lan, J. Raman Spectrosc. 40, 1791 (2009).
[43]L. Gong, R. J. Young, I. A. Kinloch, I. Riaz, R. Jalil, and K. S. Novoselov, ACS Nano 6, 2086 (2012).
[44]I. Srivastava, R. J. Mehta, Z.-Z. Yu, L. Schadler, and N. Koratkar, Appl. Phys. Lett. 98, 063102 (2011).
[45]A. Falin, Q. Cai, E. J. G. Santos, D. Scullion, D. Qian, R. Zhang, Z. Yang, S. Huang, K. Watanabe, T. Taniguchi, M. R. Barnett, Y. Chen, R. S. Ruoff, and L. H. Li, Nat. Commun. 8, 15815 (2017).
[46]T. Jiang, R. Huang, and Y. Zhu, Adv. Funct. Mater. 24, 396 (2014).